Thermal and structural properties of iron at high pressure by molecular dynamics

Kostadin G Gaminchev*

Institute of Solid State Physics, Bulgarian Academy of Sciences, 72 Tzarigradsko Chaussée blvd., 1784 Sofia, Bulgaria

We investigate the basic thermal, mechanical and structural properties of body centered cubic iron (α–Fe) at several temperatures and positive loading by means of Molecular Dynamics simulations in conjunction with the embedded-atom method potential and its modified counterpart one. Computations of its thermal properties like average energy and density of atoms, transport sound velocities at finite temperatures and pressures are detailed studied as well. Moreover, there are suggestions to obtain hexagonal close-packed structure (ε-phase) of this metal under positive loading. To demonstrate that, one can increase sufficiently the pressure of simulated system at several temperature's ranges; these structural changes depend only on potential type used. The ensuring structures are studied via the pair radial distribution functions (PRDF) and precise common-neighbor analysis method (CNA) as well.

1 Introduction

Iron is a transition metal that form the backbone of materials for buildings, vehicles and tools. Furthermore it is the most abundant element in the Earth's core. One of the most common key problems is connected to the study of thermal, mechanical as well as structural properties of the metal in order to gain insight into its phase diagram. Since the antiquity, many researchers have studied the phase stability of the iron's allotropes under different conditions.

Cooling down liquid iron, under atmospheric conditions, one obtains a body-centered

*gaminchev@issp.bas.bg

cubic (bcc) crystal at about 1811 K. At even lower temperatures the metal transforms into a face-cubic centered (fcc) approximately at 1667. By further decreasing the temperature a bcc phase sets in at a temperature of the order of 1185 K (for more details we redirect the interested reader to references [1, 2] and references therein). Besides the above mentioned structural properties, it is important to note the magnetic nature of iron. At low temperatures below Fe exhibits a ferromagnetic ordering, that vanishes at about 1043 K, called the Curie point, leaving behind a paramagnetically disordered phase [3].

Under sufficiently high external pressure iron transforms into a hexagonal-close packed (*hcp*) structure, known as ε-phase [4, 5, 6, 7]. At extremely high temperatures and pressures, such as in the earth's core, the crystallographic structure of Fe is not yet known, under these conditions some authors speculate about the existence of the so-called β-phase of iron. If such a phase exists it would set in around 1500 K and a pressure as high as 50 GPa. Its structure is supposed to be orthorhombic or double *hcp* [2]. The description of such structural transformations and the construction of the phase diagram in the temperature and pressure plane is challenging from both the theoretical and the experimental points of view.

Computer simulations, such as *ab initio*, relying on quantum–mechanical treatments give accurate results for a number of physical properties, such as lattice parameter, cohesive energies and are able to determine the phonon dispersion of the system under study. These approaches are very demanding in terms of computational resources and remains restricted to relatively small systems. To be able to gain deeper insights into the collective behavior of larger systems over longer times scales, it is preferable to use empirical interatomic potentials [8, 9, 10, 11, 12, 13, 14, 15, 16] in conjunction with simulations based upon classical methods like Molecular dynamics or Monte Carlo simulations. Usually these potentials include many-body interactions that take into account the local density profile of the material under consideration. In this study, we present compre-

hensive simulative results for elemental iron obtained from classical EAM, firstly introduced by Daw and Baskes [17, 18]. For a review see reference [8, 9, 12, 13, 14, 15, 16] and references therein. In the present work we investigate some physical properties of iron at high temperature and pressure with the help of three embedded atom interatomic potentials proposed in the Literature [13, 12, 16]. Here we will use the following notation EAM1 [13], EAM2 [12] and MEAM [16] to denote them. We are interested mainly in finding the phase structural behavior predicted by these models depending in the temperature pressure phase diagram.

The present paper is devoted to the computation via MD of some physical properties: (a) thermal – energy per atom, temperature, and pressure dependent density; (b) mechanical – sound velocities and (c) structural transformations – α-ε phase transition estimation in iron under positive loading at high temperatures whenever it is possible. It is structured as follows: in Section 2 we explain the main theoretical methods in simulation terms. The results from these procedures are discussed in Section 3. Conclusion remarks are draw on in the last Section 4.

2 Theory and computational techniques

In the current implementation for *bcc*-iron we consider a theory where the total energy of the system is given by an expression within the embedded atom method potential [17, 18]. It includes a many-body interaction term and it is used in conjunction with the MD simulation in the canonical (NVT) and isobaric-isothermal (NPT) thermodynamic ensembles. In various simulations we are using boxes with different number of atoms, depending on the particular problem, including bcc-conventional [100] and bcc-primitive unit cells. Periodic boundary conditions are imposed in all three spatial dimensions, i.e. all atoms are replicated by a period of the lattice parameter. integration time step for integrating the Newton equations of motion was chosen to be $\Delta t = 2.5$ fs to ensuring total energy conservation for all trajectories. In the NVT ensemble, simula-

tions are equilibrated at the target temperature for 2000 time steps which is necessary to obtain a stationary values for constant total energy and volume fluctuations. After equilibrating the system we compute averages over the subsequent 10^5 steps. The pair radial distribution function (PRDF), which determines the probability of finding an atom at given distance from a reference one is given by

$$g(r) = \frac{1}{4\pi N \varrho r^2 \Delta r} \left\langle \sum_i n_i \right\rangle, \quad \text{and moreover} \qquad \lim_{r\to\infty} g(r) \to 1, \tag{1}$$

where n_i is the number of atoms in a spherical region with radius r and a spherical shell Δr, while ϱ is the density of atoms inside the considered region. N is the number of steps in the molecular dynamics simulation. In equation (1) the expression in brackets $\langle ... \rangle$ means thermodynamic averaged quantities.

3 Results and discussion

Starting with a *bcc*-primitive unit cell, replicated 8 times in all space directions,we worked in the NPT ensemble for the quest of a possible α–ε phase transition. Depending on the potential, at a specific fixed temperature, the pressure was increased gradually. To obtain accurate results for both temperature and pressure of the system was equilibrated for the first 2×10^4 steps and averages were computed latter on.

In figure 1 we show possible phase transitions from *bcc* to *hcp* iron under isotropic positive loading for the *bcc*-primitive unit cell. Phase coexistence of a γ–ε phases seems to exist for all three potential types but at different values of the pressure at particular temperatures *i.e.* the phase boundaries in the (T,P)-plane for the three potentials do not coincide. At all temperature and for both EAM potentials [13, 12] the pressure is slowly increasing with the temperature. While at higher temperatures the behavior of the pressure is different, since the potential EAM2 shows a change of the P-slope accompanied by pronounced increase over 900 K. On the other hand the MEAM potential [16] seems

predicts a higher pressure than both EAM potentials in the low temperature region. At high enough T (up to ≈ 860 K) the pressure vanishes, figure 1.

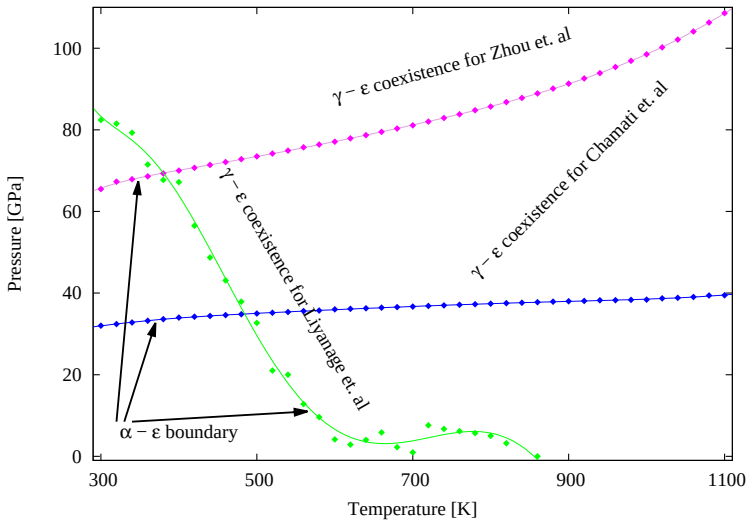

Figure 1: (Color on-line) Phase diagram of the $\alpha - \varepsilon$ phase of iron obtained via simulation with different potentials; blue diamonds [13], magenta filled circles [12] and green triangles [16]; solid lines are fitting curves. There is a stable α–phase below the simulation curves and a coexistence of $\varepsilon - \gamma$-phases above.

The structure of iron under extreme conditions, such those in the Earth's core, may be looked into by computing the averaged RDF throughout the simulation time. In figure 2 we present the computed RDFs for the different potentials, at three distinct points each, on the (T,P) phase transitions, where we believe the hcp phase is stable. The corresponding points are listed in table 1. The results depicted on figure 2 show clearly that the system has indeed an hcp structure for both EAM potentials. For the MEAM potential we found that the RDF corresponding to (400 K, 67.2 GPa) does not order neither in hcp nor bcc or fcc. It is rather plausible that in this case we have a combination of different proportions of structural domains corresponding to locally ordered structures. To guide the eye, at the bottom of the figure, we show the PDFs of the distinct structures that might be present in the material for the three potentials.

Table 1: Values of temperature and pressure used to obtain RDFs depicted in figure 2.

Potential	T [K]	P [GPa]	T [K]	P [GPa]	T [K]	P [GPa]
EAM1	400	34.40	700	36.7	1000	39.45
EAM2	400	70.0	700	81.1	1000	108.6
MEAM	400	67.2	700	0.95	1000	≈ 0.00

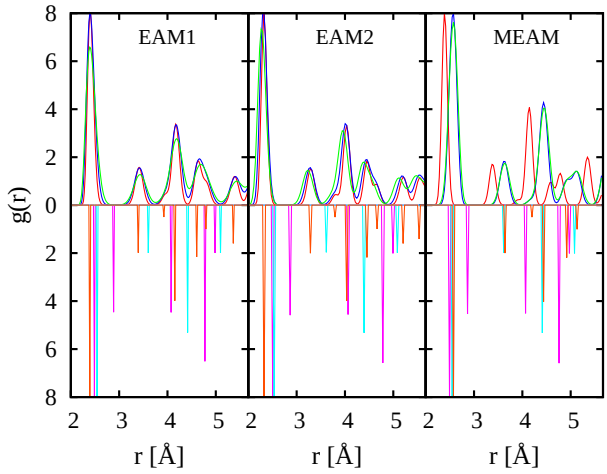

Figure 2: (Color on-line) RDFs of iron under high pressure and high temperature for potentials: EAM1 [13], EAM2 [12] and MEAM [16]; 400 K – red, 700 K – blue, 1100 K – green, compared to bcc (violet), fcc (turquoise) and hcp (orange) structures at 0 K and 0 GPa

To get an idea on how fast a phase transformation occurs from a cubic lattice to an hcp one, we applied the common neighbor analysis (CNA) method proposed in reference [19] for a series of configurations taken from the trajectories of atoms during the simulation process. So, starting from a cubic lattice at 400 K and some specific values of the pressure for each potential we could follow how the system evolves. Our results, shown in table 2, indicate clearly that the phase change sets is at different times for the three models and it is the fastest for MEAM followed by EAM2. This could be related to the set parameters that entered in constructing the potentials used here.

The mechanical and elastic properties of iron at particular temperatures and pressures corresponding to the hcp phase in the (T,P) phase diagram show quite good agree-

Table 2: CNA in percents of bcc, fcc, hcp and other unknown structures for α-ε at various stages, $\Delta\tau$, of the transformation process.

Potential	T [K]	P [GPa]	bcc [%]	fcc [%]	hcp [%]	other [%]	$\Delta\tau$ (ps)
EAM1 [13]	400	34	12.3	0.0	87.1	0.6	5.25
EAM2 [12]	400	70	5.3	0.0	88.5	6.2	1.00
MEAM [16]	400	67.2	0.2	0.0	94.7	5.1	0.5

ment among each other except for MEAM potential [16] where some components of the sound velocity give inharmonious values, table 3. It must be pointed that increasing the temperature for MEAM potential lowers the pressure of the system and at approximately 860 K the system transforms immediately in ε-γ phase and above this temperature the system becomes unstable (figure 1). Experimental results evidence show that ε-phase of iron is in wide range of pressures [20, 7] and references therein.

Table 3: Mechanical and thermal structure changes in iron under positive loading. Average sound velocities v_{ij} (km/s), velocity of compressional (P)–wave anisotropy v_{Δ_P}, energy/atom E_a(eV) as well the density $\overline{\rho}$ (kg/m^3) are computed according to three different potential types. The pressure tensor P correspond to the phase diagram in figure 1 at particular temperatures.

T [K]	P [GPa]	v_{11}	v_{12}	v_{33}	v_{44}	v_{66}	v_{Δ_P}	E_a	$\overline{\rho}$
EAM1 [13]									
300	32.0	412.9	210.3	233.1	121.9	251.3	0.565	-4.139	8949
500	35.0	427.0	231.3	239.3	122.5	253.8	0.56	-4.061	8964
700	36.7	430.2	237.7	239.5	122.4	253.6	0.557	-4.022	8939
900	38.0	433.4	245.4	241.8	123.6	252.6	0.558	-3.984	8910
1100	39.45	436.2	251.8	242.2	123.4	251.9	0.555	-3.945	8881
EAM2 [12]									
300	66.5	444.9	274.6	252.3	121.1	247.5	0.567	-3.707	9946
500	73.5	448.9	284.0	258.6	122.2	245.8	0.576	-3.617	10079
700	81.1	456.8	292.2	264.4	119.9	248.2	0.579	-3.521	10219
900	91.3	436.4	287.5	260.8	129.7	232.2	0.598	-3.403	10530
1100	108.6	463.6	303.5	266.8	153.1	247.8	0.575	-3.225	10855
MEAM [16]									
300	82.4	476.0	260.6	278.2	202.1	281.6	0.584	-3.578	9927
500	32.7	472.7	112.9	263.5	239.4	324.6	0.557	-4.037	8772
700	0.95	428.6	—	247.8	256.2	335.0	0.578	-4.106	7742

4 Conclusions

We use two of the most common EAM [13, 12] as well as a MEAM [8] interaction potential types to study high-pressure phase transition in iron under several temperature ranges from 300 K up to 1100 K. We have built the corresponding phase diagrams of the above mentioned potentials. Furthermore the CNA analysis proved that α-ε transition occurs at the corresponding pressures, that are different for each potential.

Mechanical properties like elastic moduli and sound velocities as well as thermal ones, such as average energy and density per atom are computed at selected temperatures and positive loading. The potentials used in our simulations show similar behavior, except for MEAM potential. In future work we try to build more precise and compact phase diagram based on different computer simulation methods.

Acknowledgements

The author also is grateful to Ling Ti Kong for fruitful comments. This work was supported by EU FP7 INERA project grant agreement number 316309.

References

[1] J. H. Nguyen, N. C. Holmes, Nature 427 (2004) 339–342. doi:10.1038/nature02248.

[2] R. Boehler, Rev. Geophys. 38 (2000) 221–245. doi:10.1029/1998RG000053.

[3] C. Kittel, Introduction to solid state physics, 8 ed., Wiley, New York, 2005.

[4] L. Stixrude, R. E. Cohen, D. J. Singh, Phys. Rev. B 50 (1994) 6442–6445. doi:10.1103/PhysRevB.50.6442.

[5] M. Ekman, B. Sadigh, K. Einarsdotter, P. Blaha, Phys. Rev. B 58 (1998) 5296–5304. doi:10.1103/PhysRevB.58.5296.

[6] T. Schickling, J. Buenemann, F. Gebhard, L. Boeri, Phys. Rev. B 93 (2016) 205151. doi:10.1103/PhysRevB.93.205151.

[7] N. A. Zarkevich, D. D. Johnson, Phys. Rev. B 91 (2015) 174104. doi:10.1103/PhysRevB.91.174104.

[8] M. I. Baskes, Phys. Rev. B 46 (1992) 2727–2742. doi:10.1103/PhysRevB.46.2727.

[9] M. I. Mendelev, S. Han, D. J. Srolovitz, G. J. Ackland, D. Y. Sun, M. Asta, Philos. Mag. 83 (2003) 3977–3994. doi:10.1080/14786430310001613264.

[10] M. S. Daw, S. M. Foiles, M. I. Baskes, Mater. Sci. Rep. 9 (1993) 251–310. doi:10.1016/0920-2307(93)90001-U.

[11] X. Zhou, H. Wadley, R. Johnson, D. Larson, N. Tabat, A. Cerezo, A. Petford-Long, G. Smith, P. Clifton, R. Martens, T. Kelly, Acta Mater. 49 (2001) 4005–4015. doi:10.1016/S1359-6454(01)00287-7.

[12] X. W. Zhou, R. A. Johnson, H. N. G. Wadley, Phys. Rev. B 69 (2004) 144113. doi:10.1103/PhysRevB.69.144113.

[13] H. Chamati, N. Papanicolaou, Y. Mishin, D. Papaconstantopoulos, Surf. Sci. 600 (2006) 1793–1803. doi:10.1016/j.susc.2006.02.010.

[14] A. Stukowski, B. Sadigh, P. Erhart, A. Caro, Model. Simul. Mater. Sci. Eng. 17 (2009) 075005. doi:10.1088/0965-0393/17/7/075005.

[15] B. Jelinek, S. Groh, M. F. Horstemeyer, J. Houze, S. G. Kim, G. J. Wagner, A. Moitra, M. I. Baskes, Phys. Rev. B 85 (2012) 245102. doi:10.1103/PhysRevB.85.245102.

[16] L. S. I. Liyanage, S.-G. Kim, J. Houze, S. Kim, M. A. Tschopp, M. I. Baskes, M. F. Horstemeyer, Phys. Rev. B 89 (2014) 094102. doi:10.1103/PhysRevB.89.094102.

[17] M. S. Daw, M. I. Baskes, Phys. Rev. Lett. 50 (1983) 1285–1288. doi:10.1103/PhysRevLett.50.1285.

[18] M. S. Daw, M. I. Baskes, Phys. Rev. B 29 (1984) 6443–6453. doi:10.1103/PhysRevB.29.6443.

[19] A. Stukowski, Model. Simul. Mater. Sci. Eng. 18 (2010) 015012. doi:10.1088/0965-0393/18/1/015012.

[20] D. Yamazaki, E. Ito, T. Yoshino, A. Yoneda, X. Guo, B. Zhang, W. Sun, A. Shimojuku, N. Tsujino, T. Kunimoto, Y. Higo, K.-i. Funakoshi, Geophys. Res. Lett. 39 (2012) n/a–n/a. doi:10.1029/2012GL053540.